Detection of Moving Targets in Wideband SAR

MATS I. PETTERSSON
Swedish Defence Research Agency

A likelihood ratio is proposed for moving target detection in a wideband (WB) synthetic aperture radar (SAR) system. WB is defined here as any systems having a large fractional bandwidth, i.e., an ultra wide frequency band combined with a wide antenna beam. The developed method combines time-domain fast backprojection SAR processing methods with moving target detection using space-time processing. The proposed method reduces computational load when sets of relative speeds can be tested using the same clutter-suppressed subaperture beams. The proposed method is tested on narrowband radar data.

Manuscript received February 1, 2001; revised June 3, 2003 and January 16, 2004; released for publication April 5, 2004.

IEEE Log No. T-AES/40/3/835879.

Refereeing of this contribution was handled by L. M. Kaplan.

Author's address: FOI, Olaus Magnus Väg 42, Universitetsområdet, Box 1165, SE-581 11 Linköping, Sweden, E-mail: (matsp@foi.se).

I. INTRODUCTION

A technique is described for detecting moving targets in a wideband (WB) synthetic aperture radar (SAR) system. Work on a Fourier-based WB SAR moving target detection technique has been published by Soumekh [1]. The approach presented here differs from Soumekh's work in two ways. First, our approach puts the moving target detection into the image formation process. Second, the image formation process is accomplished using a fast backprojection based approach. The goal of our approach is to both provide the extreme motion compensation needed in a WB SAR system and reduce the computational load. These benefits will occur in both processing stationary targets and focusing moving targets at different relative speeds [2].

Focusing a moving target in WB SAR is a difficult problem. In a WB SAR system, the integration time is long and thus the moving target may perform nonlinear motions and rotations during the integration time. Here we consider only targets that perform linear motion over the integration interval. Still, the results demonstrated here can be applied to any target over pieces of the aperture where the target motion can be approximated as linear.

While Fourier-based image formation approaches provide good image quality for non-WB SAR systems, they often fail to provide adequate quality imagery in WB SAR systems, because of the long integration times needed. These large integration times impose stringent demands on the motion compensation needed to form imagery in these systems. Thus time-domain backprojection algorithms, whose origins stem from global backprojection (GBP) [3, 4], are better suited for forming images in a WB SAR system.

Two examples of WB SAR systems are CARABAS^{TM} and LORA what are being developed at the Swedish Defense Research Agency (FOI) [5–7]. CARABAS is a VHF (20–90 MHz) system while LORA is a dual band system with VHF (20–90 MHz) and UHF (200–800 MHz). LORA is the next generation of low frequency radar being developed at FOI. The design of LORA is based upon CARABAS technology but extends system capabilities through both a larger bandwidth and including a UHF multi-channel antenna array. The low frequencies used by these systems, combined with their high relative resolution, provide a unique capability of detecting targets concealed in foliage [8–11]. The capabilities of the LORA system will be extended based upon the theory developed here.

There is a need to detect moving targets in WB SAR. Especially there is a need to combine time-domain SAR processing techniques with moving target detection. The work presented here addresses this problem. In Section II we discuss

time-domain image processing methods and how the movement of the target affects the target appearance. In Section IIA we review different SAR time domain processing methods, and in Section IIB we review the local backprojection (LBP) SAR image formation algorithm. In Section IIC we determine the moving target location in the SAR image. Section IID shows how a moving target can be focused using backprojection results calculated for ground speed.

In Section III we consider the antenna arrays spatial separations of the channels, and how the separation affects the location of the moving target. In Section IV we show how the antenna array in WB SAR can be used to detect moving targets in strong clutter. In Section IVA we give a review in the field and in Section IVB we develop a method to detect moving targets with a WB SAR system. The method is a combination of backprojection and space-time processing, and it is derived from a likelihood ratio test (LRT). In Section VI the method is tested on narrowband radar data, because there were no WB data available.

II. FAST BACKPROJECTION METHODS AND MOVING TARGETS IN A WB SAR SYSTEM

There are many different SAR image formation algorithms. The choice of algorithm is dependent on system configuration, available processing power, computer memory, and required quality of the resulting image. In WB SAR systems, it has been found that time-domain backprojection algorithms have good performance [11] due to the capability to handle the extreme range migration and motion compensation requirements associated with the wide antenna aperture.

A. Fast Backprojection Methods

Due to the extreme computational demands of the GBP for large images, approximate yet faster time-domain algorithms have been developed. The domain of different fast backprojection methods (FBPMs) can be categorized based upon the number of stages used in the processing. Two-stage FBPM algorithms include LBP [12] and the fast backprojection algorithm (FBPAs) [13]. Multi-stage FBPM algorithms include quadtree backprojection (QBP) [14], the FBPM mentioned in [15] and fast factorized backprojection (FFBP) [16].

For a SAR image with N aperture points and an N by N image area, the number of operations needed for GBP is proportional to N^3 while two-stage algorithms are proportional to $N^2\sqrt{N}$ and multiple-stage algorithms are proportional to $N^2\log(N)$ [14–16]. Thus QBP and FFBP have the same computational load as Fourier-domain techniques. FFBP is often preferred to QBP because the resulting image quality using FFBP can be controlled using parameter fed into the algorithm.

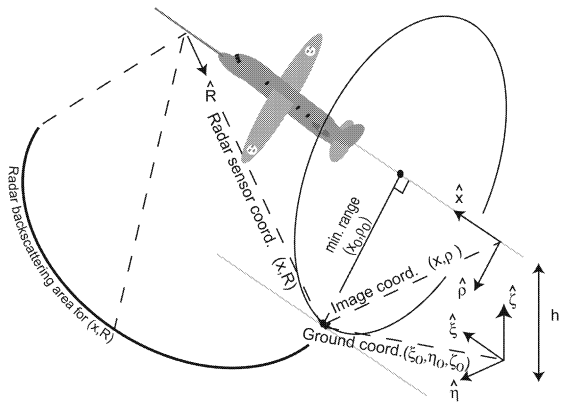

Fig. 1. The three used coordinate systems. Ground coordinate system (ξ,η,ζ), radar coordinate system (x,R) with x cross range and R range, and image coordinate system for stationary target (x,ρ).

While FFBP is often the preferred FBPM, it is not used in this work. The motive here is to provide a proof of concept of combining FBPMs with moving target detection, not optimized with respect to speed. Thus the similarities in each of the FBPMs allows us to select any approach in order to demonstrate our concept. Here the LBP algorithm was chosen over FFBP since LBP is easier to derive mathematically.

B. The LBP

Consider Fig. 1. A point target at ground position (ξ_0,η_0,ζ_0) will appear in the radar coordinate system (x,R) at different ranges given by the radar position x. Assuming a straight flight track the range migration will be a hyperbola. In the following we relate the radar coordinates to the target by the minimum range, that is when the distance between the target and the platform antenna is minimum and it is in radar coordinates given when $(x,R)=(x_0,\rho_0)$. For a nonmoving target at $(\xi_0,\eta_0,0)$ the minimum range is $\rho_0=\sqrt{\eta_0^2+h^2}$ and $x_0=\xi_0$. The backprojection process places the nonmoving target at point (x_0,ρ_0) in the image. Assume the radar antenna moves along a linear track alongside the x-axis. The output from the radar sensor for a point target at (x,R) is given by

$$\frac{p\left(R-\sqrt{(x-x_0)^2+\rho_0^2}\right)}{(x-x_0)^2+\rho_0^2} \tag{1}$$

where $p(R)$ is the compressed pulse of a point target. From the radar output we form the signal

$$g(x,R)=\frac{p\left(R-\sqrt{(x-x_0)^2+\rho_0^2}\right)}{\sqrt{(x-x_0)^2+\rho_0^2}}. \tag{2}$$

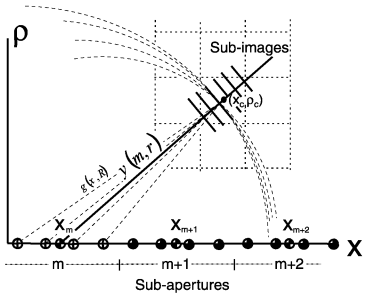

Fig. 2. Subimages and subapertures in LBP. Radar output $g(x,R)$ is sampled at $\oplus$. From radar samples, supaperture beams are calculated at every $\oplus$ (subaperture center position x_m) over each subimage. At x_m subaperture beam $y(m,r)$ is formed over subimage with center coordinate (x_c,ρ_c).

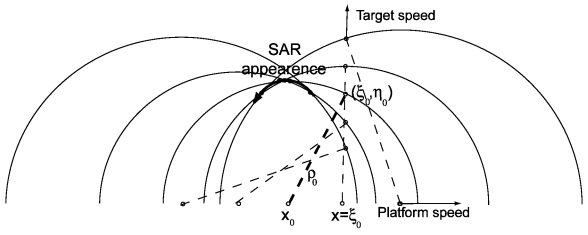

Fig. 3. Displacement and defocusing of moving target in SAR image processed for stationary targets [7]. At each radar position x there will be a location of the moving target (ξ,η). Target and platform location at five points are shown and their connected distance. At one particular point x_0 the minimum distance ρ_0 occurs. The figure is geometrical illustration that moving target will be unfocused and displaced at point (x_0,ρ_0).

We have assumed the start-stop approximation [17] to be valid, which is reasonable in an airborne system. For GBP we define the backprojected signal $h(x,\rho)$ according to

$$h(x,\rho)=\int_{-\infty}^{\infty} g\left(x',\sqrt{(x'-x)^2+\rho^2}\right)dx'. \tag{3}$$

This is a SAR image found by solving the backprojection signal (3) for each image point (x,ρ). It can be shown that the exact inversion for a point target in a system with infinite bandwidth is found after filtering $h(x,\rho)$ with a ramp filter in wave domain [4, 16]. The filtering is simply a multiplication between the wave domain transformed backprojection signal and the wave domain ramp [16]. The ramp filter lowers the sidelobes in the WB image. The interested reader can find more details about GBP in [3], [4], [12], [15], and [16].

Consider a target response located in a subimage with center coordinates ρ_c and x_c as seen in Fig. 2. In LBP the integral (3) is solved approximately over M subapertures with size L_s over one subimage. The subimage and subaperture are chosen sufficiently small such that the range distance can be approximated as a linear function. The LBP at (x,ρ), for a point target in (x_0,ρ_0), is given by

$$h(x,\rho)=\sum_{m=1}^{M}\int_{(x_m-L_s/2)}^{(x_m+L_s/2)} g \times\left(x',R_{cm}+\frac{((x'-x_m)-(x-x_c))(x_m-x_c)+(\rho-\rho_c)\rho_c}{R_{cm}}\right)dx' \tag{4}$$

where $R_{cm}=\sqrt{(x_c-x_m)^2+\rho_c^2}$ and x_m is the center coordinate in each subaperture. In LBP the subimages and subaperture size L_s are sufficiently small such that the subaperture integral dependence on (x,ρ) in a subimage over a subaperture appears as linear range shift in $g(\cdot,\cdot)$. If we form the local range history $r=(x-x_c)(x_c-x_m)+(\rho-\rho_c)\rho_c/R_{cm}$ we are able to rewrite the subaperture integral to

$$y(r,m)=\int_{(x_m-L_s/2)}^{(x_m+L_s/2)} g\left(x',R_{cm}+r+\frac{x_m-x_c}{R_{cm}}(x'-x_m)\right)dx' \tag{5}$$

which is called the subaperture beam. Also, for a particular subaperture m, the subintegral depends only upon the local range. The LBP can then be rewritten in terms of subaperture beams as

$$h(x,\rho)=\sum_{m=1}^{M} y\left(\frac{(x-x_c)(x_c-x_m)+(\rho-\rho_c)\rho_c}{R_{cm}},m\right). \tag{6}$$

Simulations of (4)–(6) are given in [2] and [18].

C. Displacement of Moving Targets in SAR Image

A moving target is displaced and unfocused in the SAR image as shown in [19] and in Fig. 3. The location where the moving target appears in the SAR image is associated with the radar coordinates of minimum range (x_0,R) where $R=\rho_0$ [6, 7]. As in [1] we change the image coordinate system so that the moving target is stationary resulting in the transformed platform velocity being the relative speed between the platform and the target velocities. To ease both the image formation process and detection, we chose the moving target parameterization to be connected to the minimum range in the radar coordinates rather than the selected origin of the coordinate system as in [1]. Because the range history is the same in all coordinate systems in Fig. 1, the displacement in a WB SAR system can be found from the distance relation between image coordinates and ground coordinates. This relationship can be written as

$$\sqrt{\gamma^2(x(t)-x_0)^2+\rho_0^2}=\sqrt{(x(t)-\xi(t))^2+\eta^2(t)+h^2}. \tag{7}$$

Here, γ is the relative speed, ξ and η are ground coordinates of the moving target, and h is the flight

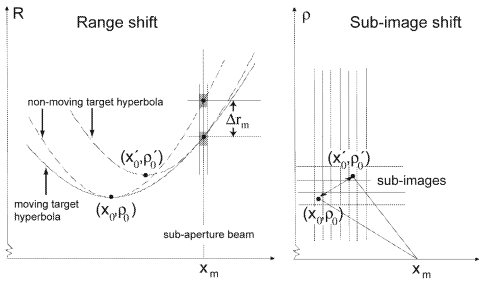

Fig. 4. Focusing with relative speed γ using subbeams calculated for ground speed. Location of moving target at (x_0, ρ_0) in subaperture x_m can be found from position (x_0', ρ_0'). If moving target speed is large there will be subimage shift during long integration.

altitude. We assume linear motion of the platform $x(t) = v_p t$, and of the moving target position $\xi(t) = v_\xi(t - t_0) + \xi_0$, $\eta(t) = v_\eta(t - t_0) + \eta_0$. The time t_0 is the time when the minimum range occurs. The moving target will be located at $(\xi_0, \eta_0, 0)$ when the antenna is at the minimum range position x_0. All coordinates x_0, ξ_0, η_0 and the time t_0 are then connected to the minimum range ρ_0, and they can easily be found for any linear motion. Combining the distance relation in (7) with the linear motion assumption gives

$$\gamma^2 = \frac{(v_p - v_\xi)^2 + v_\eta^2}{v_p^2} \tag{8}$$

$$x_0 = \xi_0 - \frac{v_\eta}{v_p - v_\xi}\eta_0 \tag{9}$$

$$\rho_0 = \sqrt{\eta_0^2\left(1 + \left(\frac{v_\eta}{v_p - v_\xi}\right)^2\right) + h^2}. \tag{10}$$

D. Focusing Moving Targets

To focus a moving target, the relative speed of that target must be taken into account in the SAR image formation process [6, 19]. To apply LBP we must recompute the subaperture beams and the image formation. To avoid this we propose a method to focus SAR images at γ using subaperture beams processed for ground speed, i.e., $\gamma = 1$.

In LBP, (6), we sum subaperture beams over the hyperbola in (x_0, ρ_0), as seen in Fig. 4. If the target is moving we can still find the moving target hyperbola in the subaperture beams processed for $\gamma = 1$. However, this requires distance compensation. In addition, if the target moves fast enough, a subimage shift will occur between adjacent subimages. An expression for this change in target position is now developed.

Assume a moving target with minimum range ρ_0 at x_0, as shown in Fig. 4. To find the subimage and range shift at x_m, we compute a point (x_0', ρ_0'), chosen such that the subaperture beam over this virtual nonmoving target is the same as the moving target at (x_0, ρ_0). Equating the range and range-derivative for the moving and virtual nonmoving target gives

$$\sqrt{\gamma^2(x_m - x_0)^2 + \rho_0^2} = \sqrt{(x_m - x_0')^2 + \rho_0'^2} \tag{11}$$

$$(x_m - x_0') = \gamma^2(x_m - x_0). \tag{12}$$

Solving (11) and (12) gives x_0' and ρ_0' as functions of x_m, x_0, ρ_0 and γ. The distance shift for a subaperture beam is given by

$$\Delta r_m = \sqrt{(x_m - x_0)^2 + \rho_0^2} - \sqrt{(x_m - x_0')^2 + \rho_0'^2}. \tag{13}$$

For moving targets with high speed and long integration time, Δr_m will change sufficiently such that the point (x_0', ρ_0') moves from one subimage to a neighboring subimage. A subimage shift occurs when this happens.

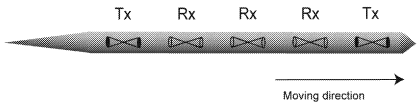

Fig. 5. LORA antenna with two transmitting channels (Tx) and three receiving channels (Rx).

III. FAST BACKPROJECTION AND MOVING TARGETS IN A WB SAR SYSTEM WITH AN ANTENNA ARRAY

To detect a moving target an antenna array often used. This section describes how the locations of the antenna channel affect the results derived in Section II. In this article we propose an along track array similar to the antenna developed for LORA, Fig. 5. Because there will be bistatic measurements between the transmitting antenna and the receiving antennas we define an effective antenna phase center. The effective antenna center approximates the bistatic wave from two displaced antennas as a monostatic wave from one antenna located in the middle of the transmitting and receiving antenna. How this approximation affects SAR processing and moving target detection is given in [1] and [33]. Also the antenna configuration has a total of L channels and the separation between the first effective antenna center to the effective antenna center of channel l is d_l.

In Section IIB the LBP was derived for one antenna channel. If we add more channels in an antenna array we have to take into consideration the different locations of the phase center of the channels. LBP can easily handle the bistatic wave originated in the array antenna, so in the processing there is no need to compensate the bistatic wave according to [1] and [33]. The subaperture given for channel l in (5) is

given by

$$y_l(r,m) = \int_{(x_m - L_s/2 + d_l)}^{(x_m + L_s/2 + d_l)} g_l\left(x', R_{cm} + r + \frac{x_m - x_c}{R_{cm}}(x' - x_m)\right) dx' \tag{14}$$

for each of the L channels in the radar system. The LBP can then be rewritten in terms of subaperture beams for channel l as

$$h_l(x,\rho) = \sum_{m=1}^{M} y_l\left(\frac{(x - x_c)(x_c - x_m) + (\rho - \rho_c)\rho_c}{R_{cm}}, m\right). \tag{15}$$

In Section IIC we gave the displacement of the moving target in one antenna channel in (8)–(10). In an antenna array the moving target will change its position between the channels, due to the connection between space and time associated with a moving platform. We now investigate how the moving target changes its location in the other antenna channels. The amount of change by the target in each channel is given by the time difference when the minimum range occurs in the spatially separated antenna channels. If the distance between the effective antenna phase center for channel l to the first antenna channel is d_l, the separation time Δt_l is found from (7) to be

$$\Delta t_l = \frac{d_l(v_p - v_\xi)}{(v_\xi - v_p)^2 + v_\eta^2}. \tag{16}$$

For stationary targets, the time difference between the channels will be the time it takes for the platform to move from the two effective antenna centers.

From the separation time, the moving target minimum range can be found for each channel by using (8)–(10). The point where the minimum range occur in radar coordinates is separated for each channel to first channel by

$$\Delta x_{0l} = \frac{(v_p - v_\xi)}{v_p \gamma^2} d_l. \tag{17}$$

For a stationary target (17) gives the distance d_l between the effective antenna centers which is expected. The minimum range will in each channel be separated by

$$\Delta\rho_{0l} = \sqrt{\rho_0^2 + \frac{2\eta_0 d_l v_\eta}{(v_p - v_\xi)} + \frac{d_l^2 v_\eta^2}{(v_p - v_\xi)^2 + v_\eta^2}} - \rho_0 \approx \frac{\eta_0 d_l v_\eta}{\rho_0(v_p - v_\xi)} \tag{18}$$

where the approximation is valid when $d_l \ll 2\eta_0$ and $|2d_l v_\eta| \ll |\rho_0(v_p - v_\xi)|$ which is true for almost all SAR radar cases with a fast platform and a target moving on ground. From the minimum range in the radar coordinate system it is easy to find target positions using the image coordinate system given by the first channel $(\gamma' x_0, \rho_0)$, where γ' is the used processing speed in image formation. However, in the other channels the SAR images are considering the spatial separation of the channels so the SAR image appearance will be $(\gamma'(x_0 + \Delta x_{0l} - d_l), \rho_0 + \Delta\rho_{0l})$ and for stationary target $\gamma = 1$ processed at ground speed $\gamma' = 1$ the position will in all channels be (x_0, ρ_0).

IV. MOVING TARGET DETECTION

A. Introduction to Moving Target Detection in SAR

Moving target detection in radar has been well studied for many years. Detection of moving targets requires maximization of the target signal compared with the clutter. To filter moving targets from strong clutter the displaced-phase-center-antenna (DPCA) method was developed [21]. This technique needs strict spatial alignment and system stability. As an extension of an adaptive antenna technique in [22] the space-time adaptive processing (STAP) approach was developed for ground moving target indicator (GMTI) [23]. STAP is not only adaptive but can also be used for slow moving target detection. The effectiveness of STAP with GMTI is because the clutter spectrum is normally restricted to a narrow ridge in two-dimensional space-time [24, 25], which is well separated from the position of moving targets.

In recent years GMTI has developed in combination with SAR. In a SAR GMTI system the moving target will not only be detected but also imaged in its surroundings. Movement of a target will have an effect on the focus of the target in the SAR image relative to it surroundings. To suppress clutter multi-channel antenna arrays can be used. An overview of SAR GMTI is given in [26]. The main detection scheme is the likelihood ratio test (LRT) [27–30]. Experimental results [31–32] have confirmed that these SAR GMTI techniques are a strong tool to detect and image moving targets in its surrounding.

B. Likelihood Ratio Test for Moving Target Detection in Fast Backprojection

The geometry of the SAR platform and the moving target is given in Fig. 6. The speed of the target is given by the speed v_t and heading α, and we assume linear motion on a flat plane. The moving target will appear in the subaperture beam connected to φ and range. The true angle to the moving target is given by φ'.

In WB systems, it is a benefit to use subaperture beams processed for ground speed [2, 18]. Sub aperture beams allows for frequency and angle dependent mismatch in the system as well as to save processing load and reduce data complexity. This aids in the performance of moving target detection.

The illuminated area is divided into subimages, connected to subapertures through subaperture beams

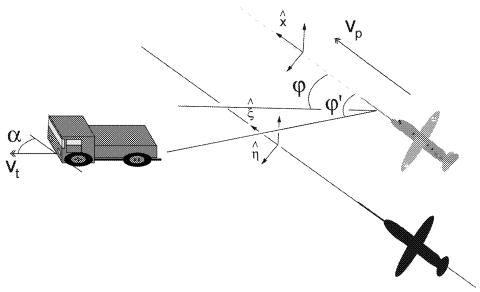

Fig. 6. Moving target heading and speed in ground coordinate system $(v_\xi, v_\eta, 0) = v_t(\cos\alpha, \sin\alpha, 0)$. Direction from plane to moving target is φ'. Subaperture beams are formed according to Doppler and moving target will appear in subaperture at direction φ.

$y_l(r,m)$. If a moving target is present, the subaperture beams consist of a moving target $z_l(r,m)$, clutter $q_l(r,m)$ and white noise independent of direction $n_l(r,m)$. The clutter and the noise are considered to be independent. The clutter is connected to the radar backscattering while the noise originates from thermal noise in the system. These two are independent. The subaperture beam $y_l(r,m)$ under the two hypotheses, $\mathbf{H_0}$ no target present and, $\mathbf{H_1}$ target present are

$$\mathbf{H_0}: \quad y_l(r,m) = a_l^c(r,m) * q_l(r,m) + n_l(r,m) \tag{19}$$

$$\mathbf{H_1}: \quad y_l(r,m) = a_l^t(r,m) * z_l(r,m) + a_l^c(r,m) * q_l(r,m) + n_l(r,m) \tag{20}$$

for the antenna channels $l = 1,\ldots,L$, where $*$ is the convolution with respect to r, $a_l^c(r,m)$ is the system response to the clutter, and $a_l^t(r,m)$ is the system response to the target. Functions $a_l^c(r,m)$ and $a_l^t(r,m)$ differ, because of the different origin directions of the target and the clutter. The measurements in the radar system will be sampled signals, thus in the following we use the sampled subaperture beam with vector components $y_l(r_\mu,m)$, where r_μ is the sample points in local range given by $r_\mu = r_0 + \Delta r_s \mu$, where r_0 is a constant offset, Δr_s is the sampling interval, and μ is the sampling index from 0 to $N-1$.

Experience from WB jammer suppression in the CARABAS system (which is a WB system) indicates that the moving target detection should be done in the frequency domain [20]. The wave-transformed subaperture beams (according to r) in LBP are located in SAR image wave number space and seen in Fig. 7. Using subaperture beams it is convenient to express the wave number vector $\mathbf{k}$ in a polar coordinate system with radius $k = \sqrt{k_\rho^2 + k_x^2}$ and k_φ (the same angle as φ in Fig. 6 in means of stationary phase [33]). In the radial direction in wave domain we have N samples, and M subapertures in angular direction, the index are n and m, respectively.

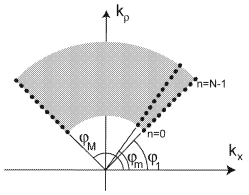

Fig. 7. Wave number space. Subaperture beams are located in image wave number space.

The received signal under the two hypotheses $\mathbf{H_0}$ and, $\mathbf{H_1}$ in wave number space is

$$\mathbf{H_0}: \quad \tilde{y}_l(\mathbf{k}) = \tilde{a}_l^c(\mathbf{k})\tilde{q}_l(\mathbf{k}) + \tilde{n}_l(\mathbf{k}) \tag{21}$$

$$\mathbf{H_1}: \quad \tilde{y}_l(\mathbf{k}) = \tilde{a}_l^t(\mathbf{k})\tilde{s}_l(\mathbf{k})e^{j\phi(\mathbf{k})}e^{-j(r(\mathbf{k})+(l-1)\Delta(\mathbf{k}))k} + \tilde{a}_l^c(\mathbf{k})\tilde{q}_l(\mathbf{k}) + \tilde{n}_l(\mathbf{k}) \tag{22}$$

for $l = 1,\ldots,L$ and where $\mathbf{k}$ is the wave number vector dependent on the wave number k and subaperture m (dependent on Doppler angle φ), $\tilde{a}_l^c(\mathbf{k})$ is the wave function of the system in the clutter direction, $\tilde{a}_l^t(\mathbf{k})$ is the wave function of the system in the target direction, $\tilde{s}_l(\mathbf{k})$ is the target scattering amplitude, $\phi(\mathbf{k})$ is the phase of the target scattering, $r(\mathbf{k})$ is the local range of the target in the subaperture in first channel, $\Delta(\mathbf{k})$ denotes the movement of the target in local range between the spatial channels, and the sum $r(\mathbf{k}) + (l-1)\Delta(\mathbf{k})$ is the target local range in channel l. For simplicity, we have in the following assumed equally separated channels, with a distance d between effective antenna centers given $d_l = (l-1)d$.

The measurement vector in wave number space, for all L channels and all sampled wave transformed subaperture beams, is an L–N–M vector

$$\tilde{\mathbf{Y}} = \begin{bmatrix} \tilde{y}_1(k_0,\varphi_1) \\ \tilde{y}_2(k_0,\varphi_1) \\ \vdots \\ \tilde{y}_L(k_0,\varphi_1) \\ \tilde{y}_1(k_1,\varphi_1) \\ \vdots \\ \tilde{y}_L(k_{N-1},\varphi_1) \\ \vdots \\ \tilde{y}_L(k_{N-1},\varphi_M) \end{bmatrix} = \begin{cases} \tilde{\mathbf{q}} + \tilde{\mathbf{n}} & \text{under } \mathbf{H_0} \\ \tilde{\tilde{\mathbf{A}}} + \tilde{\mathbf{q}} + \tilde{\mathbf{n}} & \text{under } \mathbf{H_1} \end{cases} \tag{23}$$

where $\tilde{\mathbf{q}}$ and $\tilde{\mathbf{n}}$ are the clutter and noise vectors, respectively. The antenna pattern in a WB SAR system is very broad and therefore the antenna changes slowly with angle. The antenna changes will probably be small between $\tilde{a}_l^t(\mathbf{k})$ and $\tilde{a}_l^c(\mathbf{k})$. In this paper we assume all antennas have the same

gain in all directions and that there are no frequency dependencies in the system, i.e., $\tilde{a}_l^t(\mathbf{k}) = \tilde{a}_l^c(\mathbf{k}) = 1$. The signal vector is then given by

$$\tilde{\tilde{\mathbf{A}}} = \begin{bmatrix} e^{j\phi(k_0,\varphi_1')}s(k_0,\varphi_1')e^{-jk_0 r_1^t} \\ e^{j\phi(k_0,\varphi_1')}s(k_0,\varphi_1')e^{-jk_0(r_1^t+d(\cos\varphi_1-\cos\varphi_1'))} \\ \vdots \\ e^{j\phi(k_0,\varphi_1')}s(k_0,\varphi_1')e^{-jk_0(r_1^t+(L-1)d(\cos\varphi_1-\cos\varphi_1'))} \\ e^{j\phi(k_1,\varphi_1')}s(k_1,\varphi_1')e^{jk_1 r_1^t} \\ \vdots \\ e^{j\phi(k_{N-1},\varphi_1')}s(k_{N-1},\varphi_1')e^{-jk_{N-1}(r_1^t+(L-1)d(\cos\varphi_1-\cos\varphi_1'))} \\ \vdots \\ e^{j\phi(k_{N-1},\varphi_M')}s(k_{N-1},\varphi_M')e^{-jk_{N-1}(r_M^t+(L-1)d(\cos\varphi_M-\cos\varphi_M'))} \end{bmatrix}. \tag{24}$$

According to Section IID the moving target will perform a range history in the subapertures r_m^t given by minimum range and (13).

To test for the presence of a target, we use the LRT, written mathematically as

$$\Lambda = \frac{P(\tilde{\mathbf{Y}} \mid \mathbf{H_1})}{P(\tilde{\mathbf{Y}} \mid \mathbf{H_0})}. \tag{25}$$

The probability density function (pdf) of the noise $n_l(r_\mu, m)$ is assumed Gaussian. The resolution cell in each radar output $g_l(x,R)$ is large compared with the center wavelength and for that reason the resolution cell contains many scatterers. Still in the subaperture beams $y_l(r_\mu, m)$ the resolution cell is large compared with the wavelength. With a high probability there are still many scatterers in the resolution cell of the subaperture beam. It is then appropriate to model the $q(r_\mu, m)$ pdf as Gaussian [34], as a consequence of the central limit theorem. The transformation from range to wave domain of a sequence is a summation, and a summation of Gaussian variables is a Gaussian variable. Therefore we use Gaussian pdfs for the clutter $\tilde{\mathbf{q}}$ and noise $\tilde{\mathbf{n}}$. Then under $\mathbf{H_0}$:

$$P(\tilde{\mathbf{Y}} \mid \mathbf{H_0}) = \frac{1}{(2\pi)^{NM}|\tilde{\mathbf{C}}|} e^{-\tilde{\mathbf{Y}}^H \tilde{\mathbf{C}}^{-1}\tilde{\mathbf{Y}}} \tag{26}$$

and under $\mathbf{H_1}$:

$$P(\tilde{\mathbf{Y}} \mid \mathbf{H_1}) = \frac{1}{(2\pi)^{NM}|\tilde{\mathbf{C}}|} e^{-(\tilde{\mathbf{Y}}-\tilde{\tilde{\mathbf{A}}})^H \tilde{\mathbf{C}}^{-1}(\tilde{\mathbf{Y}}-\tilde{\tilde{\mathbf{A}}})} \tag{27}$$

where $\tilde{\mathbf{C}}$ is the covariance matrix of $\tilde{\mathbf{Y}}$

$$\tilde{\mathbf{C}} = E[(\tilde{\mathbf{q}} + \tilde{\mathbf{n}})(\tilde{\mathbf{q}} + \tilde{\mathbf{n}})^H]. \tag{28}$$

If we assume a moving point target we can simplify the measurement signal. The amplitude s_0, and phase ϕ_0, of a point target are independent of direction and frequency. The amplitude of the measured signal thus depends only upon range and is approximately the subaperture center range R_{cm}. The phase ϕ_0 is random and distributed uniformly between 0 and 2π. Under the point target approximation the signal vector can be expressed as

$$\tilde{\tilde{\mathbf{A}}} = s_0 e^{j\phi_0}\tilde{\mathbf{A}} \tag{29}$$

where $\tilde{\mathbf{A}}$ is the steering vector given by

$$\tilde{\mathbf{A}} = \begin{bmatrix} \dfrac{e^{-jk_0 r_1^t}}{R_{c1}^2} \\ \dfrac{e^{-jk_0(r_1^t+d(\cos\varphi_1-\cos\varphi_1'))}}{R_{c1}^2} \\ \vdots \\ \dfrac{e^{-jk_0(r_1^t+(L-1)d(\cos\varphi_1-\cos\varphi_1'))}}{R_{c1}^2} \\ \dfrac{e^{jk_1 r_1}}{R_{c1}^2} \\ \vdots \\ \dfrac{e^{-jk_{N-1}(r_1^t+d(\cos\varphi_1-\cos\varphi_1'))}}{R_{c1}^2} \\ \vdots \\ \dfrac{e^{jk_{N-1}(r_M^t+(L-1)d(\cos\varphi_M-\cos\varphi_M'))}}{R_{cM}^2} \end{bmatrix}. \tag{30}$$

Since ϕ_0 is random, the LRT is given by

$$E_\phi[\Lambda(\tilde{\mathbf{Y}})] = \int_0^{2\pi} \Lambda(\tilde{\mathbf{Y}} \mid \phi_0)\frac{d\phi_0}{2\pi}. \tag{31}$$

According to [35] the test variable is

$$|\tilde{\mathbf{A}}^H \tilde{\mathbf{C}}^{-1}\tilde{\mathbf{Y}}|^2 \begin{cases} > \lambda & \text{decision for } \mathbf{H_1} \\ < \lambda & \text{decision for } \mathbf{H_0} \end{cases}. \tag{32}$$

The clutter noise and the receiver noise can be considered as independent, giving

$$\tilde{\mathbf{C}} = E[\tilde{\mathbf{Y}}\tilde{\mathbf{Y}}^H] = E[\tilde{\mathbf{q}}\tilde{\mathbf{q}}^H] + E[\tilde{\mathbf{n}}\tilde{\mathbf{n}}^H]. \tag{33}$$

The receiver noise samples $n_l(r_\mu, m)$ are independent both in local range r_μ and in between antenna channels l. The clutter signal $q_l(r_\mu, m)$ is dependent in l, but independent in m and r_μ. The subaperture beams are formed by nonoverlapping samples which are independent, i.e., independent looks [34]. The wave number transformation will cause dependency on wave number k_n both for $\tilde{q}_l(k_n, \varphi_m)$ and $\tilde{n}_l(k_n, \varphi_m)$. However, if the number of radial samples N is sufficiently large then the dependency in k_n is weak [36], thus we assume the samples to be independent.

The covariance will then simplify to

$$\tilde{\mathbf{C}} = \begin{bmatrix} \bar{\mathbf{C}}_{01} & 0 & \cdots & 0 & 0 & \cdots & 0 \\ 0 & \bar{\mathbf{C}}_{11} & \cdots & 0 & 0 & \cdots & 0 \\ \vdots & \vdots & \ddots & \vdots & \vdots & \cdots & \vdots \\ 0 & 0 & & \bar{\mathbf{C}}_{(N-1)1} & 0 & \cdots & 0 \\ 0 & 0 & \vdots & 0 & \bar{\mathbf{C}}_{12} & \cdots & 0 \\ \vdots & \vdots & \vdots & \vdots & \vdots & \ddots & \vdots \\ 0 & 0 & 0 & 0 & 0 & \cdots & \bar{\mathbf{C}}_{(N-1)M} \end{bmatrix} \tag{34}$$

where the diagonal matrixes $\bar{\mathbf{C}}_{nm}$ are given by

$$\bar{\mathbf{C}}_{nm} = E[\bar{\mathbf{q}}_{nm}\bar{\mathbf{q}}_{nm}^H] + E[\bar{\mathbf{n}}_{nm}\bar{\mathbf{n}}_{nm}^H] \tag{35}$$

and where the clutter $\bar{\mathbf{q}}_{nm}$ and the noise $\bar{\mathbf{n}}_{nm}$ are indexed in the same way as the measurement vector $\bar{\mathbf{Y}}_{nm}$, given by

$$\bar{\mathbf{Y}}_{nm} = \begin{bmatrix} \tilde{y}_1(k_n, \varphi_m) \\ \tilde{y}_2(k_n, \varphi_m) \\ \vdots \\ \tilde{y}_L(k_n, \varphi_m) \end{bmatrix}. \tag{36}$$

The LRT is now reduced to

$$|\tilde{\mathbf{A}}^H\tilde{\mathbf{C}}^{-1}\tilde{\mathbf{Y}}|^2 = \left|\sum_{m=1}^{M}\sum_{n=0}^{N-1}\bar{\mathbf{A}}_{nm}^H\bar{\mathbf{C}}_{nm}^{-1}\bar{\mathbf{Y}}_{nm}\right|^2 = \begin{cases} > \lambda & \text{decision for } \mathbf{H_1} \\ < \lambda & \text{decision for } \mathbf{H_0} \end{cases} \tag{37}$$

and the steering vector simplifies to

$$\bar{\mathbf{A}}_{nm} = \frac{e^{-jk_n r_m^t}}{R_{cm}^2}\begin{bmatrix} 1 \\ e^{-jk_n d(\cos\varphi_m - \cos\varphi_m')} \\ \vdots \\ e^{-jk_n(L-1)d(\cos\varphi_m - \cos\varphi_m')} \end{bmatrix} = \frac{e^{-jk_n r_m^t}}{R_{cm}^2}\bar{\bar{\mathbf{A}}}_{nm}(\varphi_m') \tag{38}$$

and the LRT can be written as

$$|\tilde{\mathbf{A}}^H\tilde{\mathbf{C}}^{-1}\tilde{\mathbf{Y}}|^2 = \left|\sum_{m=1}^{M}\frac{1}{R_{cm}^2}\sum_{n=0}^{N-1}e^{jk_n r_m^t}\bar{\bar{\mathbf{A}}}_{nm}^H(\varphi_m')\bar{\mathbf{C}}_{nm}^{-1}\bar{\mathbf{Y}}_{nm}\right|^2 = \left|\sum_{m=1}^{M}\frac{1}{R_{cm}^2}y_c(r_m^t, m, \varphi_m')\right|^2 = \begin{cases} > \lambda & \text{decision for } \mathbf{H_1} \\ < \lambda & \text{decision for } \mathbf{H_0} \end{cases} \tag{39}$$

using the notation

$$y_c(r, m, \varphi_m') = \sum_{n=0}^{N-1}e^{jk_n r_m^t}\bar{\bar{\mathbf{A}}}_{nm}^H(\varphi_m')\bar{\mathbf{C}}_{nm}^{-1}\bar{\mathbf{Y}}_{nm}. \tag{40}$$

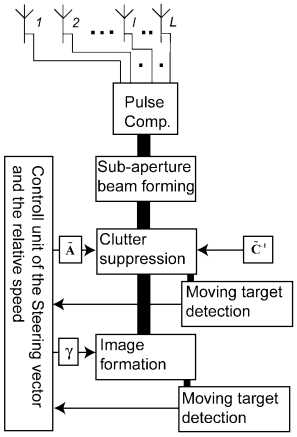

Fig. 8. Moving target detection scheme. After pulse compression, subaperture beams are formed at ground speed for each antenna channel (Section IIB and Section III). Clutter-suppressed subaperture beams are formed by L subaperture beams by covariance and the target steering vector (Section IVB). Clutter-suppressed subaperture beams are combined during image formation considering relative speed (Section IID). Moving target can be detected using only one clutter-suppressed subaperture beam and to increase the detectability the beams are combined in image formation (Section IV).

The vector $\bar{\mathbf{Y}}_{nm}$ includes the antenna channels at one wave domain point n and m. The product $\bar{\bar{\mathbf{A}}}_{nm}^H(\varphi_m')\bar{\mathbf{C}}_{nm}^{-1}\bar{\mathbf{Y}}_{nm}$ will maximize the ratio between the target to clutter and noise [23]. Because clutter is correlated and often much stronger than the thermal noise we call it clutter suppression. The multiplication with $e^{jk_n r}$ and a summation in n is a transformation to time-domain. In the following we call $y_c(r, m, \varphi_m')$ the clutter-suppressed subaperture beam. More details about (40) are given in Appendix A. In the LRT, the sum of $y_c(r_m^t, m, \varphi_m')$ in m is computed for the target location r_m^t and the angle φ_m' to test if a moving target with speed v_t and heading α is present at minimum distance (x_0, ρ_0).

In words the LRT in (25) is performed to test if a target is present at (x_0, ρ_0) with speed v_t and heading α. First the subaperture beams for all channels are formed at ground speed. There will be L subaperture beams, for each subaperture and each subimage. For the moving target there will be one clutter-suppressed subaperture beam $y_c(r_m^t, m, \varphi_m')$ at each subaperture m. The needed subaperture beams to compute $y_c(r_m^t, m, \varphi_m')$ and the target location r_m^t are found considering relative speed, γ, according to Section IID. The next step is to combine the $y_c(r_m^t, m, \varphi_m')$ across m in (39). For each m the ratio between the target to clutter and noise will increase, and therefore the summation in m will increase the delectability.

Fig. 8 demonstrates the moving target test. The clutter suppression stage computes the clutter-suppressed subaperture beams $y_c(r_m^t, m, \varphi_m')$. These beams are combined over all available subapertures M, and is called the image formation,

in Fig. 8. The figure also indicates the possibility to detect moving targets in $y_c(r_m^t, m, \varphi_m')$ using only one subaperture m, which is used in the experimental data in Section VI.

To test for other moving targets, the clutter-suppressed subaperture beam has to be computed for each target and each m. Thus target detection is done though a filter bank referring to the target velocity vector, which can be justified mathematically by the likelihood test. However if the target appears in the same subaperture beam as other targets the covariance and the subaperture beams can be reused, which saves computation.

In this paper we have assumed an ideal target that performs linear motion over the entire integration time and we can use all M clutter suppressed subaperture beams available. For real targets the approximation of linear motion is dependent on platform motion, target motion, and radar parameters. In many real situations the linear approximation is not valid over the long integration time associated with a WB system. However the number of used clutter-suppressed subaperture beams in (39) is tunable and can be optimized to the situation. Therefore (39) can be used piecewise over the large aperture.

V. EXPERIMENTAL DATA

The method described in Section III is developed for a WB SAR system. Because there are no multi-channel, WB data available, we, tested the algorithms on a narrowband data set. The narrowband data set will give an insight into the WB method performance. The data used set comes from the C-band Andover radar system, developed by the SAR group in the Defence Evaluation Research Agency (DERA) in Malvern, United Kingdom.

The radar system operates at 5.7 GHz with a frequency bandwidth of 82 MHz and an antenna beamwidth of 8 deg. The system is able to digitally record fully coherent multiple phase center radar data with VV polarization and a pulse repetition frequency (PRF) of 1.25 kHz. The radar consists of two side-looking antennas displaced 0.49 m in the along track direction. Both antennas are used as receivers and transmitters and the system alternates transmitting between the leading and trailing antennas. This gives the system a total of 4 channels: channel A, Tx front Rx front; channel B, Tx front Rx back; channel C, Tx back Rx front, and channel D, Tx back Rx back. The antenna phase center location will change between the channels. For channel A the phase center will be at the leading antenna, for channel D the phase center will be at the trailing antenna; while channels B and C have a phase center approximately half way in between the front and back antenna. The clutter leakage caused by this approximation is negligible [33].

The data set used is from Porton Down in England and was collected in November 1995. In this set there is one military vehicle moving along a tree lined track with a speed of 4–5 m/s in the across track direction and an unknown target with unknown speed and direction.

To illustrate the experimental data for one channel we form three small images by a frequency transform in slow time. These are shown in Fig. 9. The images are formed over approximately 0.2 s at the slow time positions 500, 1750, and 3000, with a Fourier transform length of 256 samples. In all images the clutter has an offset in Doppler, which is caused by the narrow antenna beam pointing forward in the flight direction. The moving target is not separated from the clutter at 500, but at 1750 one of the moving targets is at the edge of the clutter signal, and at 3000 the two targets are well separated from the Doppler signal. The known military vehicle is at far range while an unknown vehicle is in near range. The different Doppler speeds of the moving target and the clutter cause the moving targets to separate from the clutter. We now test the proposed method to this data set.

VI. TARGET DETECTION IN DERA DATA

DERA provided four-channel pulse-compressed radar data for these analyses. From these, ground speed processed subaperture beams where formed for each antenna channel. The antenna center, not the ground, was chosen as reference point due to the lack of high quality positioning data. The subaperture length and subimage size were selected in order to satisfy the far field approximation. The geometry of the subaperture and the subbeams are given in Fig. 10.

For target detection we used the method described in Section IV. In real data we do not know the target position (x_0, ρ_0), speed v_t, and heading α. Therefore we have to test many different possibilities in these parameters. In this data set with no high quality positioning data we have chosen to test without the summation of subapertures m i.e., $M = 1$. To test if a target is present in direction φ' at subaperture angle φ we form a subaperture beam $y_c(r, 1, \varphi')$. By a fast Fourier transform (FFT) of $\bar{\bar{\mathbf{A}}}_n^H(\varphi')\bar{\mathbf{C}}_n^{-1}\bar{\mathbf{Y}}_n$ in n we are able to test if there is a target present for all possible r.

The proposed method uses the subaperture beams in the frequency domain and the statistics of the noise and the clutter signal. To estimate the statistics we divided the range samples in the subaperture beams into eight range bins, according to Fig. 10. These bins where transformed to the frequency domain. Under the assumption that the clutter signal is much stronger than the target signal, the covariance was estimated between the channels by the maximum likelihood

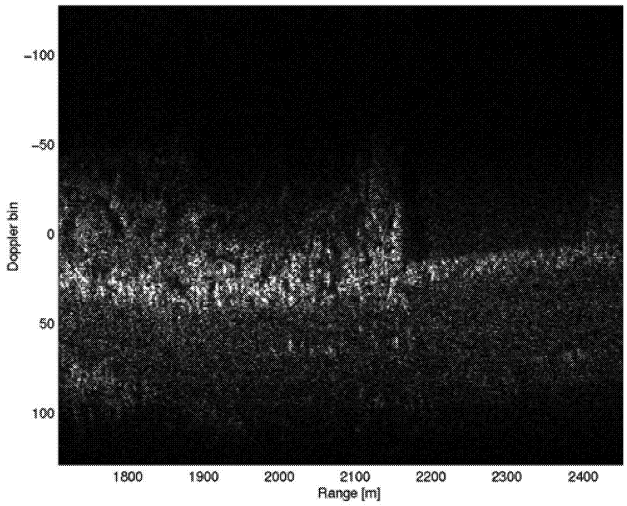

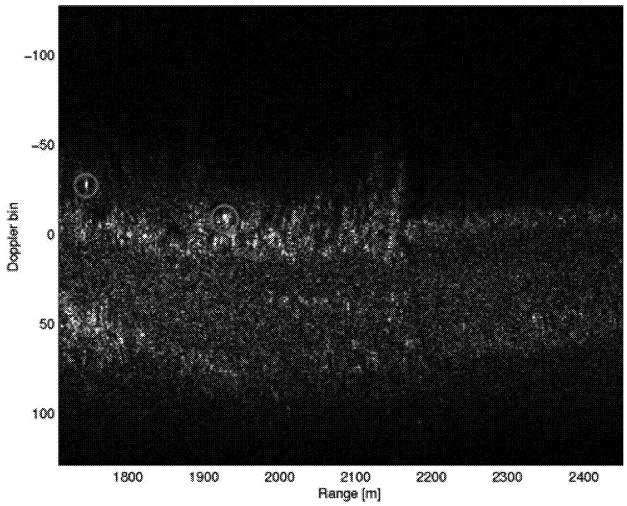

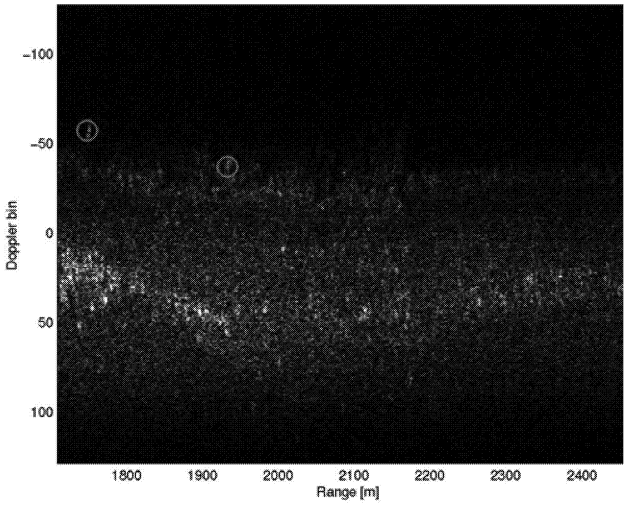

Fig. 9. Doppler-range images. Two moving targets appear clearly when they are well separated in Doppler from clutter.

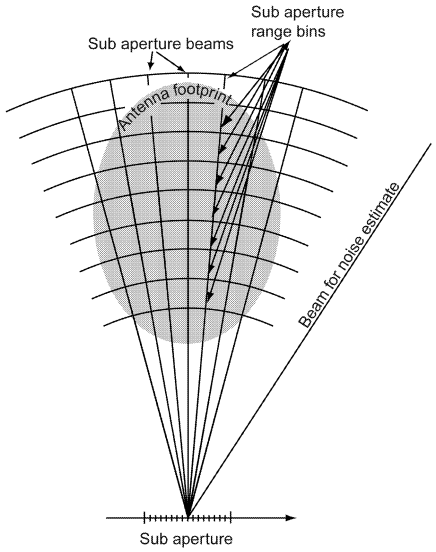

Fig. 10. Subaperture beams connected to one subaperture and antenna footprint. Each subaperture beam for each channel over antenna footprint was divided into range bins used to estimate the covariance matrix. One subaperture beam was formed over smallest antenna gain for noise estimate to CNR.

estimate of the covariance

$$\bar{\mathbf{C}}_n^p = E[\bar{\mathbf{Y}}_n^p \bar{\mathbf{Y}}_n^{p^H}] \approx \frac{1}{8} \sum_{p=1}^{8} \bar{\mathbf{Y}}_n^p \bar{\mathbf{Y}}_n^{p^H} \tag{41}$$

where p is the index of the subaperture bin. The algorithm will automatically compensate for the differences between the antenna channels. Combined with (41), we used constant false alarm rate (CFAR) normalization to ensure a constant false alarm.

VII. RESULTS

To detect the moving targets in the data set we used the method described in Section IV. The selected region of slow time samples was between 0–4000 in the data set. This is an extended data set compared with that shown in images in Fig. 9. Especially, in samples 0–500 the targets are surrounded by stronger clutter than shown in the images in that figure. The subaperture beams were formed using (5) under far field approximation. The subimage size was selected to 10 m in azimuth at the range distance of 2100 m, which corresponds to an angle of approximately 0.27 deg between the beams. In Fig. 11 the subaperture beam for one antenna channel, at 250 with angle 88.08 deg, is shown. The subaperture contains a moving target. However, it is not possible to detect the moving targets due to the strong clutter.

The subaperture beams for all channels where calculated. From these beams the covariance was estimated according to (41). The clutter-suppressed subaperture beam was calculated using the covariance, the steering vector, and the computed subaperture

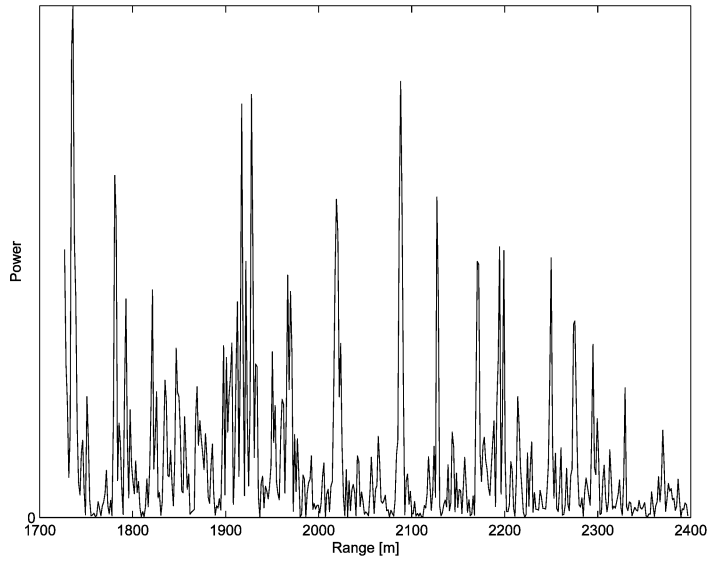

Fig. 11. Subaperture beam formed at sample 250 with angle 88.08 deg for one channel in data set. Power is in linear scale.

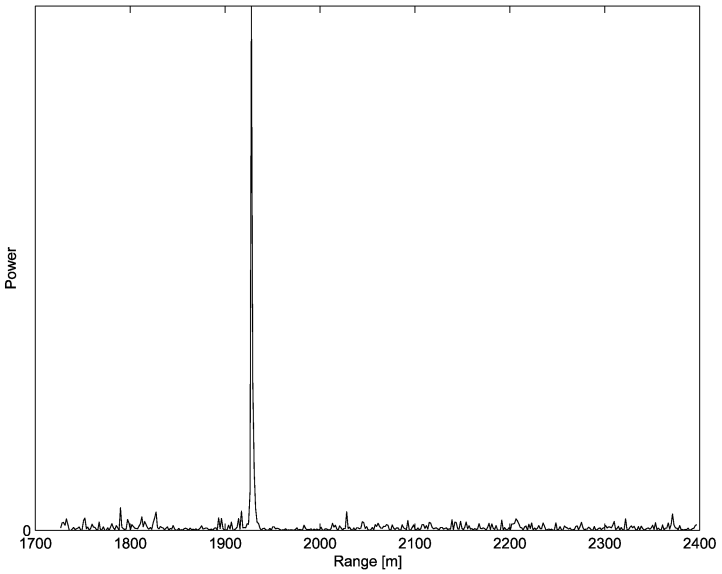

Fig. 12. Clutter-suppressed subaperture beam from Fig. 11 after clutter suppression. Clutter suppression is above 20 dB. Power is in linear scale.

beams. The clutter-suppressed subaperture beam shown in Fig. 12 is over the same area as the subaperture beam in Fig. 11. The moving target, not detectable in Fig. 11, appears clearly in the beam, and can be detected. The steering vector was selected to optimize the signal-to-clutter noise ratio (SCNR). The results of target detection from different subapertures beams are shown in Figs. 13 and 14 as a function of Doppler angle φ (Fig. 6). The unknown near-range moving target is given in Fig. 13 and the military target is given in Fig. 14. The figures give the clutter-to-noise ratio (CNR), the SCNR for one subaperture beam ($SCNR_{nf}$), and the SCNR for the clutter-suppressed subaperture beam ($SCNR_f$). The CNR is found by the ratio between the clutter estimate and the noise estimate beam in Fig. 10. The method to estimate $SCNR_f$ and $SCNR_{nf}$ is given in Appendix B. When the SCNR is small the estimate will have large uncertainty and we have used standard deviation as the confidence interval of the estimates. The derivation of the std of SCNR is provided in Appendix B. Because of the strong clutter at low Doppler angles the $SCNR_{nf}$ is very small, and the standard deviation is so large that the lower confidence limit goes to negative infinity. Therefore in Fig. 14, seven $SCNR_{nf}$ low angle measurements are averaged to one point. The average is 0.37 dB and the uncertainty of the average below 0 dB is now only 4 dB.

As seen in Figs. 13 and 14, the CNR decreases as the angle φ increases over the measured interval. The

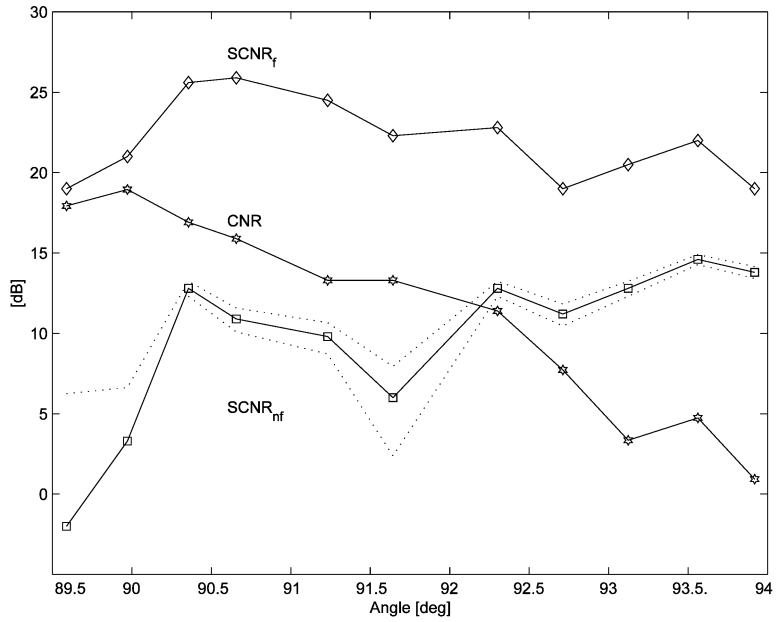

Fig. 13. Unknown moving target at range 1750 m. Three curves are $SCNR_f$, $SCNR_{nf}$, and CNR as function of Doppler angle. $SCNR_{nf}$ and $SCNR_f$ are SCNR before and after clutter suppression has been applied, respectively. Error lines of $SCNR_{nf}$ estimate are given by variance are indicated with dashed lines.

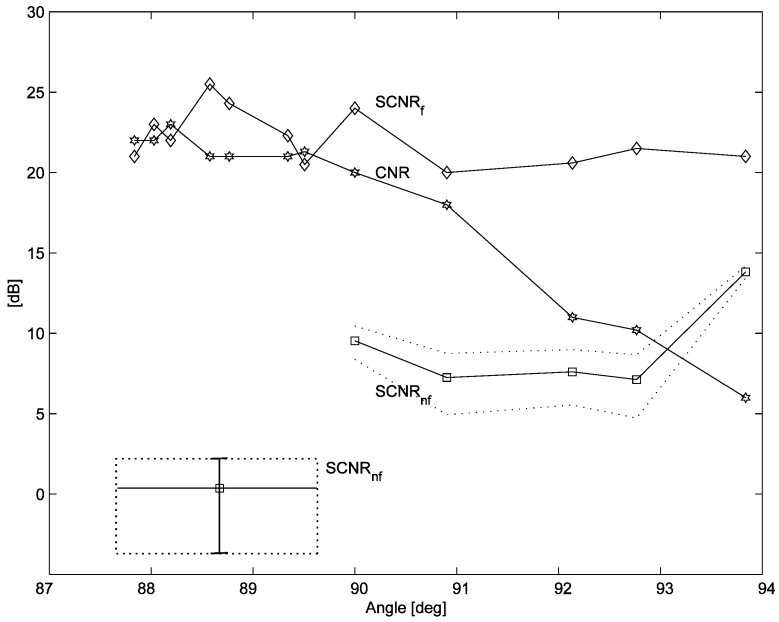

Fig. 14. Military moving target at range 1950 m. Three curves are $SCNR_f$, $SCNR_{nf}$, and CNR as function of Doppler angle. $SCNR_{nf}$ and $SCNR_f$ are SCNR before and after clutter suppression has been applied. Error lines of $SCNR_{nf}$ estimate are given by variance and are indicated with dashed lines. Due to low $SCNR_{nf}$ at low angles, seven subaperture beams are averaged to provide one $SCNR_{nf}$ estimate, which appears in dashed box in lower left-hand corner.

$SCNR_f$ is nearly stable while the $SCNR_{nf}$ increases with angle. The clutter suppression is estimated from the Figs. 13 and 14 by the ratio of $SCNR_f$ and $SCNR_{nf}$ [37]. We then use a real moving target to estimate the clutter suppression. The approach will underestimate the clutter suppression due to the fact that the $SCNR_f$ depends on target parameters, such as speed and vibrations, and radar system parameters such as system stability. If the target has a slow speed the clutter-suppression algorithm will also suppress the target.

Other authors have implemented a synthetic moving target in their SAR data to measure the clutter suppression [38, 39]. The synthetic target will be an ideal target that has a stability in scattering and motion that no real targets can achieve. The synthetic target will not be influenced by imperfections in the radar system. With a synthetic target we would

therefore overestimate the clutter suppression. For this article, we have chosen a real target which gives a proper estimate when the backscattering is strong and the target speed sufficiently high. For a $SCNR_{nf}$ around 0 dB the lower confidence limit goes towards minus infinity, which implies the $SCNR_{nf}$ is likely to be overestimated. An underestimation of $SCNR_f$ and an overestimation of $SCNR_{nf}$ means an underestimation of the clutter suppression.

The clutter suppression from Figs. 13 and 14 was found to be greater than 20 dB, and for some subapertures the suppression was 25 dB. These results are a slightly lower than the 23–30 dB reported by [32], [38], and [40]. However these papers do not describe the clutter estimate procedures, confidence, or statistical background used making comparison of these techniques difficult. For example, [38] uses synthetic moving targets as opposed to our experiments that use real targets. Real targets give an underestimation of clutter suppression. In addition performance is dependent on the test site. Note that clutter suppression is bound by the CNR, which in Figs. 13 and 14 is just over 20 dB.

VIII. DISCUSSION

To detect a moving target in a WB SAR system we combine multi-antenna channel fast backprojection SAR processing with moving target detection, by a space-time approach. There are many FBPMs, such as the ones given in Section IIA; LBP, FBPA, QBP, and FFBP. The aim of this work is to perform GMTI using the multi-stage algorithm FFBP. However, the derivation of our technique using LBP is more mathematically straight forward. Therefore we use LBP in our derivation. The results given here are also valid for FFBP.

The developed method gives the possibility of detecting moving targets, suppressing the clutter signal, and forming images of the moving target. In the algorithm we assume the target has linear motion during illumination. The quality of this approximation is dependent on platform motion, target motion, distance to target, and radar parameters such as frequency. It is probably invalid for many targets in a WB SAR system, since the more time spent illuminating the target increases the chance of nonlinear motion. However we can select a shorter integration time where the linear approximation is valid and we are free to choose the number of subapertures M used in the test (39). In particular the variable M fits very well with the multi-stage backprojection algorithms such as FFBP. In the future, further work is needed to increase the integration time and the number of clutter-suppressed subaperture beams in the test.

In the experimental data set clutter suppression was found to be approximately equal to the limit by the CNR of approximately 20 dB. The image formation phase of the clutter-suppressed subaperture beams were not implemented on the experimental data. In the data set the subapertures have a length of approximately 10 m, corresponding to approximately 0.1 s in time. In the used C-band system, a moving target will most likely have near linear motion with respect to the platform for more than 0.1 s, thus we assumed 1 s and chose $M = 10$. This will increase $SCNR_f$ and this increase is dependent on relative speed. The integration time under linear motion assumtion is dependent on radar frequency and motion of the target and platform.

IX. CONCLUSION

In this article we have presented a method for detecting moving targets in a WB SAR system with an antenna array. WB implies both an ultra wide frequency band and wide antenna beam. In WB SAR systems, time-domain backprojection has shown to be very effective. The developed method combines fast backprojection SAR processing methods with moving target detection. In FBPMs the SAR image formation process is divided into two steps, beam forming and image formation.

The LRT is found from the subaperture beams from the L channels of the antenna array. The proposed test performs clutter suppression in the subaperture beams by space-time processing and combines the clutter suppressed subaperture beams to form a test image. The combination of clutter-suppressed subaperture beams is the same as performing SAR image formation of a moving target, which requires the relative speed of the target.

The proposed target detection method forms subaperture beams at ground speed, performs clutter suppression, and finally combines the clutter suppressed subaperture beams by relative speed. This means that many different targets with different locations and speeds can be testing using the same covariance matrix and subaperture beams. This reuse of computed beams saves computational resources [2].

The proposed method assumes linear motion of the moving target over the long integration time needed in a WB SAR system. How good this approximation is depends upon the target and radar motion as well as the radar parameters such as frequency. For many situations the approximation is not good when the illuminating time for the target increases, because of the increase in chance for nonlinear motion. However, in the developed method it is possible to select pieces of the long aperture where the linear approximation can be used. To increase the resolution of the moving target, further work has to be done to increase the integration time by nonlinear motion considerations.

The proposed target detection method was developed for WB SAR systems. Unfortunately,

there are no multi-channel WB data available. Therefore the method was tested using narrowband data. The image formation, i.e., the combination of clutter-suppressed subaperture beams by relative speed, was not implemented in this data set. The results of the clutter suppressed subaperture beams indicate that clutter suppression is approximately 20–25 dB and equal to the CNR, as expected.

APPENDIX A

In (14) the subaperture beam for antenna channel l is given. Here we use the sampled subaperture beam given in vector form by

$$\mathbf{y}_l(m) = \begin{bmatrix} y_l(r_0,m) \\ y_l(r_1,m) \\ \vdots \\ y_l(r_{N-1},m) \end{bmatrix} \tag{42}$$

where r_μ is the sample points in local range given by $r_\mu = r_0 + \Delta r_s \mu$, and r_0 is a constant offset, Δr_s is the sampling interval, and μ is the sampling index from 0 to $N-1$. By the discrete wave transformation the wave transformed subaperture beam is given by

$$\tilde{y}_l(k_n,m) = \frac{1}{N}\sum_{\mu=0}^{N-1} e^{-jk_n r_\mu} y_l(r_\mu,m), \qquad n = 0,1,\ldots,N-1 \tag{43}$$

where k_n is wave domain points given by $k_n = k_0 + \Delta k_s n$, and k_0 is the lowest used wave number and $\Delta k_s = 2\pi/N\Delta r_s$. The inverse transformation is then

$$y_l(r_\mu,m) = \sum_{n=0}^{N-1} e^{jk_n r_\mu} \tilde{y}_l(k_n,m), \qquad \mu = 0,1,\ldots,N-1. \tag{44}$$

The wave transformed subaperture beam in vector form $\tilde{\mathbf{y}}_l(m)$ is given by

$$\tilde{\mathbf{y}}_l(m) = \begin{bmatrix} \tilde{y}_l(k_0,m) \\ \tilde{y}_l(k_1,m) \\ \vdots \\ \tilde{y}_l(k_{N-1},m) \end{bmatrix}. \tag{45}$$

In (40) we have the product

$$\bar{\bar{\mathbf{A}}}_{nm}^H(\varphi'_m)\bar{\mathbf{C}}_{nm}^{-1}\bar{\mathbf{Y}}_{nm} \tag{46}$$

where $\bar{\bar{\mathbf{A}}}_{nm}(\varphi'_m)$ is the steering vector given in Equation (38), $\bar{\mathbf{C}}_{nm}$ is the covariance given in (35), and $\bar{\mathbf{Y}}_{nm}$ is the measurement vector for one point in wave domain formed of the L antenna channels given in (36). At every n and m the product $\bar{\bar{\mathbf{A}}}_{nm}^H(\varphi'_m)\bar{\mathbf{C}}_{nm}^{-1}\bar{\mathbf{Y}}_{nm}$ will maximize the SCNR [23]. The product will maximize the signal described by the steering vector compared with the clutter and noise described by the covariance. In words we combine the antenna channels in $\bar{\mathbf{Y}}_{nm}$ such that we get the best possible SCNR for the target described by $\bar{\bar{\mathbf{A}}}_{nm}(\varphi'_m)$. We can then form a subaperture beam with wave components

$$\tilde{y}_c(k_n,m,\varphi'_m) = \bar{\bar{\mathbf{A}}}_{nm}^H(\varphi'_m)\bar{\mathbf{C}}_{nm}^{-1}\bar{\mathbf{Y}}_{nm} \tag{47}$$

and all n components in the subaperture m have maximized SCNR given by

$$\tilde{\mathbf{y}}_c(m) = \begin{bmatrix} \tilde{y}_c(k_0,m,\varphi'_m) \\ \tilde{y}_c(k_1,m,\varphi'_m) \\ \vdots \\ \tilde{y}_c(k_{N-1},m,\varphi'_m) \end{bmatrix} \tag{48}$$

in vector form. For a particular r in (40) we have

$$\sum_{n=0}^{N-1} e^{jk_n r} \tilde{y}_c(k_n,m,\varphi'_m). \tag{49}$$

Comparing the inverse transformation in (44) this is just a transformation from wave domain to range domain.

$$y_c(r,m,\varphi'_m) = \sum_{n=0}^{N-1} e^{jk_n r} \tilde{y}_c(k_n,m,\varphi'_m). \tag{50}$$

The range domain subaperture beam will also have maximum SCNR and we therefore call it the clutter-suppressed subaperture beam.

APPENDIX B

To analyze the performance of the GMTI method used here we need to estimate $\mathrm{SCNR_{nf}}$, $\mathrm{SCNR_f}$, and CNR. This Appendix describes how these estimates and their accuracy are determined.

The $\mathrm{SCNR_f}$ was determined from the clutter-suppressed subaperture beam using the following procedure. The peak energy from the target was determined in the clutter-suppressed subaperture beam. The clutter and noise energy $\overline{\sigma}_{CN-f}$ was found by averaging all samples, excluding the samples of the target and its surroundings. The target energy is estimated form the peak energy after subtracting $\overline{\sigma}_{CN-f}$. The $\mathrm{SCNR_f}$ was determined from the ratio between the target energy and $\overline{\sigma}_{CN-f}$.

The $\mathrm{SCNR_{nf}}$ is found in a subaperture beam connected to one antenna channel. The $\mathrm{SCNR_{nf}}$ is more complicated to estimate then $\mathrm{SCNR_f}$, due to the strong clutter surrounding the target. To find the peak value of the moving target in the subaperture beam we used the target location found in the clutter-suppressed subaperture beam. The range gate of the moving target in the clutter-suppressed subaperture beam gives the range gate in the subaperture beam, and from this the peak energy was found. The clutter and noise

energy in the subaperture beam $\overline{\sigma}_{CN-nf}$ was found in the same way as the clutter-suppressed subaperture beam. Finally the $\mathrm{SCNR}_{\mathrm{nf}}$ was computed in the same way as for $\mathrm{SCNR}_{\mathrm{f}}$ using the peak energy and $\overline{\sigma}_{CN-nf}$.

The estimate of CNR is determined from $\overline{\sigma}_{CN-nf}$ and the thermal noise, which is estimated from a subaperture beam far from the main antenna footprint, as seen in Fig. 10.

The estimate of $\mathrm{SCNR}_{\mathrm{f}}$ has high accuracy due to the large ratio (< 20 dB). However, the estimate of $\mathrm{SCNR}_{\mathrm{nf}}$ is more complicated because of the strong clutter backscattering. The unknown phase relation between target and clutter will cause a large uncertainty in the estimate. Assuming the peak method [41], the relative mean squared error of the SCNR estimate is given by

$$\varepsilon^2 = \frac{1 + \dfrac{1}{N_s}}{\mathrm{SCNR}^2} + \frac{2}{\mathrm{SCNR}} \tag{51}$$

where N_s is the number of independent clutter samples. From the relative mean squared error we get the variance and the mean. To indicate the accuracy in the estimate of SCNR a top and a bottom limit is given by the variance. The variance is estimated by using (51). When the SCNR goes below 4 dB, the relative mean squared error increases over 1. In Fig. 14 we have therefore used all independent samples of $\mathrm{SCNR}_{\mathrm{nf}}$ between 87.8 to 89.6 deg to estimate the mean and variance given in one point.

ACKNOWLEDGMENT

We would like to acknowledge, Defence Evaluation Research Agency (DERA) in United Kingdom (UK) and the UK MoD Coporate Research Programme for the C-band data. Especially the Author would like to thank Dr. Mark Williams and Darren Coe both at DERA for their help and assistance with this data set. We also acknowledge Dave Murray at NASoftware UK for processing at DERA.

The author is grateful to Adj. Professor Lars Ulander, Swedish Defence Research Institute (FOI) and Prof. Mats Viberg at Chalmers University of Technology for ideas and useful comments on this paper. The Author is also grateful to Dr. Bill Pierson, U.S. Air Force Research Laboratory (AFRL), for help with the English language in the article and to Gunnar Stenström at FOI for the transformation of the DERA data to a readable data format.

REFERENCES

[1] Soumekh, M. (1997)
Moving target detection in foliage using along track monopulse synthetic aperture radar imaging.
IEEE Transactions on Image Processing, **6** (1997), 1148–1162.

[2] Pettersson, M. I. (2000)
Focusing of moving targets in an ultra-wide band SAR GMTI system.
In *Proceedings of the 3rd Europian Conference on Synthetic Aperture Radar* (EUSAR 2000), Germany, 2000, 837–840.

[3] Fawcett, J. A. (1985)
Inversion of N-dimensional spherical averages.
SIAM Journal of Applied Mathematics, **45**, 2 (1985), 336–341.

[4] Andersson, L. E. (1988)
On determination of a function from spherical averages.
SIAM Journal of Applied Mathematics, **19**, 1 (1988), 214–341.

[5] Hellsten, H., Ulander, L. M. H., Gustavsson, A., and Larsson, B. (1996)
Development of VHF CARABAS II SAR.
SPIE Conference on Radar Sensor Technology, Vol. 2747, Orlando, FL, USA Apr. 8–9, 1996, 48–60.

[6] Hellsten, H., and Ulander, L. M. H. (1999)
Airborne array aperture UWB UHF-motivation and system consideration.
In *Proceedings of the 1999 IEEE Radar Conference* (Radar to the Next Millenium), Waltham, MA, 1999, 47–53.

[7] Ulander, L. M. H., and Hellsten, H. (1999)
Low-frequency ultra wideband array-antenna SAR for stationary and moving target imaging.
In *Proceedings of SPIE Conference on Radar Sensor Technology IV*, **3704**, Orlando, FL, 1999, 149–157.

[8] Ulander, L. M. H., Frölind, P. O., Gustavsson, A., Hellsten, H., and Larsson, B. (1999)
Detection of concealed ground targets in CARABAS SAR images using change detection.
In *Proceedings of SPIE Conference on Algorithms for Aperture Radar Imagery VI*, **3721**, Orlando, FL, 1999, 243–252.

[9] Ulander, L. M. H. (1998)
Approaching the wavelength resolution limit in ultra-wideband VHF-SAR.
In *Proceedings of the PIERS Workshop on Advances in Radar Methods*, Baveno, Italy, 1998, 83–85.

[10] Ulander, L. M. H., and Hellsten, H. (1996)
A new formula for SAR spatial resolution.
AEÜ International Journal of Electronic Communication, **50**, 2 (1996), 117–121.

[11] Ulander, L. M. H., and Frölind, P-O. (1999)
Precision processing of CARABAS HF/VHF-band SAR data.
In *Proceedings of IGARSS'99, Vol. 1*, Hamburg, Germany, 1999, 47–49.

[12] Seger, O., Herberthson, M., and Hellsten, H. (1998)
Real time SAR processing of low frequency ultra wide band radar data.
In *Proceedings of EUSAR'98*, Friedrichshafen, 1998, 489–492.

[13] Yegulalp, A. F. (1999)
Fast backprojection algorithm for synthetic aperture radar.
In *Proceedings of 1999 IEEE Radar Conference*, Waltham, MA, 1999, 60–65.

[14] McCorkle, J., and Rofheart, M. (1996)
An order $N^2 \log(N)$ backprojector algorithm for focusing wide-angle wide-bandwidth arbitary-motion synthetic aperture radar.
In *Proceedings of SPIE Conference on Radar Sensor Technology, Vol. 2947*, Orlando, FL, 1996, 25–36.

[15] Nilsson, S. (1997)
Application of fast backprojection techniques for some inverse problems of integral geometry.
Dissertation 499, Department of Mathematics, Linköping University, Linköping, Sweden, 1997, ISBN 91-7219-021-3.

[16] Ulander, L. M. H., Hellsten, H., and Stenström, G. (2003)
Synthetic-aperture radar processing using fast factorised back-projection.
IEEE Transactions on Aerospace and Electronic Systems, **39**, 3 (July 2003), 760–776.

[17] Barber, B. C. (1985)
Theory of digital imaging from orbital synthetic-aperture radar.
International Journal of Remote Sensing, **6** (1985), 1009–1057.

[18] Pettersson, M. I., Ulander, L. M. H., and Hellsten, H. (1999)
Simulations of ground moving target indication in a ultra-wideband and wide-beam SAR system.
In *Proceedings of SPIE Conference on Radar Processing, Technology and Application IV, Vol. 3810*, Denver, CO, 1999, 84–95.

[19] Raney, R. K. (1971)
Synthetic aperture imaging radar and moving targets.
IEEE Transactions on Aerospace and Electronic Systems, **AES-7**, 3 (1971), 499–505.

[20] Pettersson, M. I., and Ulander, L. M. H. (1999)
Jammer suppression in an ultra-wideband and widebeam SAR system.
Presented at the 5th International Conference on Radar Systems, Radar'99, Brest, France.

[21] Skolnik, M. I. (1970)
Radar Handbook.
New York: McGraw-Hill, 1970.

[22] Widrow, B., Mantey, P. E., Griffiths, L. J., and Goode, B. B. (1967)
Adaptive antenna systems.
Proceedings of IEEE, **55**, 12 (1967), 2143–2159.

[23] Brennan, L. E., Mallett, J. D., and Reed, I. S. (1976)
Adaptive arrays for airborne MTI radar.
IEEE Transactions on Antennas and Propargation, **24**, 5 (1976).

[24] Ward, J. (1994)
Space-time processing for for airborne radar.
Technical report 1015, Lincoln Lab, Massachusetts Institute of Technology, 1994.

[25] Klemm, R. (1998)
Space-Time Adaptive Processing; Principles and Applications, London: IEEE, 1998.

[26] Ender, J. H. G. (1999)
Space-time processing for multichannel synthetic aperture radar.
IEE Electronics & Communication Engineering Journal, 1999, 29–38.

[27] Barbarossa, S. (1992)
Detection and imaging of moving objects with synthetic aperture, Part 1: Optimum detection and parameter estimation theory.
IEE Proceedings F, (Radar and Signal Processing), **139**, 1 (1992), 79–88.

[28] Barbarossa, S., and Farina, A. (1992)
Detection and imaging of moving objects with synthetic aperture, Part 2: Joint time-frequency analysis by Wigner-Ville distribution.
IEE Proceedings F, (Radar and Signal Processing), **139**, 1 (1992), 89–97.

[29] D'Addio, E., Di Bisceglie, M., and Bottalico, S. (1994)
Detection of moving objects with airborne SAR.
EURASIP, *Signal Processing*, **3612** (1994), 149–162.

[30] Ender, J. H. G. (1993)
Detectability of slowly moving targets using a multi-channel SAR with an along-track antenna array.
SEE/IEE Colloquium on SAR-93, Paris, 1993, 18–22.

[31] Ender, J. H. G. (1998)
Experimental results achieved with the airborne multi-channel SAR system AER-II.
In *Proceedings of the European Conference on Synthetic Aperture Radar*, (EUSAR'98), Friedrichshafen, 1998, 315–318.

[32] Coe, D. J., and White, R. G. (1996)
Experimental moving target detection results from a three-beam airborne SAR.
AEÜ International Journal of Electronic Communication, **50**, 2 (1996), 157–164.

[33] Pettersson, M. I. (2001)
Extraction of moving ground targets by a bistatic ultra-wideband and -widebeam SAR system.
IEE Proceedings on Radar, Sonar and Navigation, **148**, 1 (2001), 35–40.

[34] Oliver, C., and Quegan, S. (1998)
Understanding Synthetic Aperture Radar Images.
London: Artech House, 1998.

[35] Chen, W. S., and Reed, I. S. (1991)
A new CFAR detection test for radar.
Digital Signal Processing, **1**, 4 (1991), 198–214.

[36] Ljung, L. (1999)
System Identification, Theory for the User.
Upper Saddle River, NJ: Prentice-Hall, 1999.

[37] Nathanson, F. E. (1969)
Radar Design Principles—Signal Processing and the Environment, New York: McGraw-Hill, 1969.

[38] Farina, A., Timmoneri, L., Graziana, R., and Lee, F. (1995)
Adaptive space-time processing with systolic algorithm: Experimental results using recorded live data.
Proceedings of Radar 95 (IEEE International Radar Conference), Virginia, 1995, 495–602.

[39] Farina, A., Lombardo, P., and Pirri, M. (1999)
Nonlinear STAP processing.
IEE Electronics & Communication Engineering Journal, 1999, 41–48.

[40] Stockburger, E. F., and Held, D. N. (1995)
Interferometric moving ground target imaging.
Proceedings of Radar 95 (IEEE International Radar Conference), Virginia, 1995, 495–602.

[41] Ulander, L. M. H. (1991)
Accuracy of using point targets for SAR calibration.
IEEE Transactions on Aerospace and Electronic Systems, **27**, 1 (1991).

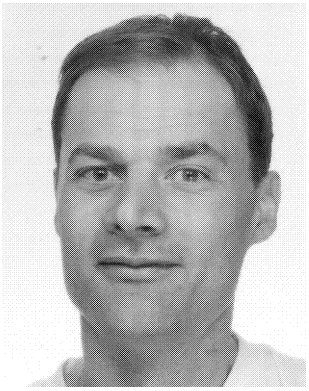

Mats I. Pettersson received his M.S. in engineering physics, in 1993 and Ph.D. in signal processing in 2000 both from Chalmers University of Technology (CTH), Gothenbourg, Sweden.

He was a Ph.D. student at Radio and Space Science CTH between 1993–1995 working with radar remote sensing. Between 1996–1997 he was at Ericsson Mobile Communication in Lund and since 1998 he has been at Swedish Defence Researh Agency (FOI) in Linköping. At FOI he is working with space-time adaptive processing in combination with SAR processing in wide band SAR systems. He research is on jammer suppression and moving target detection algorithms specially for the FOPEN systems CARABAS and LORA.